INTERFERENCE FILTERS FOR COLORED GLAZED THERMAL SOLAR COLLECTORS

A. Schüler, C. Roecker, and J.-L. Scartezzini
Laboratoire d'Energie Solaire et de Physique du Bâtiment LESO-PB, Ecole Polytechnique Fédérale de Lausanne EPFL, Bâtiment LE, 1015 Lausanne, Switzerland, tel. : *41-21-6934544, andreas.schueler@epfl.ch

J. Boudaden, I. R. Videnovic, R. S.-C. Ho, P. Oelhafen
Institut für Physik der Universität Basel, Klingelbergstr. 82, CH-4056 Basel, Switzerland

Abstract – Glazed thermal solar collectors, typically equipped with black, optical selective absorber sheets, exhibit good energy conversion efficiency. However, the black color, and sometimes the visibility of tubes and corrugations of the metal sheets, limit the architectural integration into buildings. In order to overcome this drawback, interference filters are considered as a promising approach. Multilayered thin film stacks deposited on the cover glass can produce a colored reflection hiding the black absorber without a great loss of energy. These interference filters are designed and optimized by numerical simulation. Such coatings can be deposited by vacuum processes (e.g. magnetron sputtering) or via the SolGel method. Optical measurements, such as spectrophotometry or ellipsometry, are used to determine film thicknesses and optical constants of individual layers, and to measure color coordinates and solar transmission for the multilayer stacks.

1. INTRODUCTION

Architectural integration of solar energy systems into buildings has become a widely recognized issue now (Hestnes, 1999), regarding techniques from photovoltaics and daylighting to thermal solar energy conversion. Considerable activities have demonstrated the possibilities of building integration of photovoltaic cells [(Roecker et al., 1995); (Hagemann, 2002)], leading to a large product variety, and finally enhancing crucially the user acceptance of solar cells. Daylighting elements based on anidolic mirrors have been successfully introduced into building facades in an aesthetically pleasing way (Scartezzini and Courret, 2002). Thermal solar collectors, typically equipped with black, optical selective absorber sheets, exhibit in general good energy conversion efficiencies. However, the black color, and sometimes the visibility of tubes and corrugations of the metal sheets, limit the architectural integration into buildings. Various attempts have been made to overcome this drawback. One option is to color the absorber sheets. Optical selective absorber coatings are usually deposited by processes such as magnetron sputtering [(Graf et al., 1997); (Schüler et al., 2001)], vacuum evaporation (Lazarov et al., 1995), electrochemical processes (Tabor, 1955), SolGel technology (Kaluza et al., 2001), or as selective paint (Orel and Gunde, 2001). These processes are usually optimised for high solar absorption, yielding typically black or dark blue surfaces. Modifying the process parameters can result in a colored appearance. Selective paints can be prepared to exhibit e.g. blue, green, and brownish red colors. By varying layer thicknesses, sputtered absorber coatings can also be colored in a large variety of shades. Following this approach, the absorber surface combines the functions of optical selectivity (high solar absorption/low thermal emission) and colored reflection. Tripanagnostopoulos reports a different solution: his group used non-selective colorful paints as absorber coatings for glazed and unglazed collectors, and compensated the energy losses by additional booster reflectors (Tripanagnostopoulos et al., 2000). An alternative option to solve the problem is to establish a colored reflection not from the absorber but from the cover glass. This approach has the advantage that the black, sometimes ugly absorber sheet is then hidden by the colored reflection. Additionally, the functions of optical selectivity and colored reflection are separated, giving more freedom to coating optimization. We propose to deposit a colored coating on the inner or outer side of the cover glass (or on both). This coating should reflect a color, but transmit the complementary spectrum. No absorption should occur in the coating. Meeting these requirements, interference colors of dielectric thin films are ideally suited for this purpose. Coloring the bulk glass by colors of absorption would affect mainly the transmission color, and in addition to that, energy would be lost uselessly. A lot of literature exists about multilayer interference stacks for various optics and laser applications [see (Macleod, 2001), and refs. therein], but to the knowledge of the authors only few deals with its application as energy-efficient coloration of thermal solar collectors.

In this work, we study the theoretical potential of colored solar collectors, and the simulation and design of interference filters with suitable properties. For their realization, we consider the SolGel method and reactive magnetron sputtering processes.

2. DEFINITION OF A FIGURE OF MERIT AND THEORETICAL POTENTIAL OF COLORED COLLECTORS

The International Commission on Illumination (CIE, Commission Internationale d'Eclairage) described how to quantify colors (International Commission on Illumination CIE, 1986). All existing colors can be represented in a plane and mapped by Cartesian coordinates, as shown in the CIE Chromaticity Diagrams. The quantification is based on the 1931 CIE Color Matching Functions, x(λ), y(λ), and z(λ), which reflect the color sensitivity of the human eye. These functions depend to some extent on the width of the observation field and are given for opening angles of 2° and 10°. Tristimulus values X, Y, and Z are computed from three similar integrations of the measured or simulated spectral power distribution data P(λ):

$$\begin{aligned} X &= \int P(l)\cdot x(l)dl \\ Y &= \int P(l)\cdot y(l)dl \\ Z &= \int P(l)\cdot z(l)dl \end{aligned} \qquad (1)$$

The spectral power distribution P(λ) can be, for example, the product of a source spectrum and a simulated or measured reflection spectrum of a sample. In the case of Lambertian or specular reflecting surfaces, one can work with the hemispherical reflectance R(λ). Representing typical daylight, the standard illuminant D_{65} is commonly used as a source:

$$P(l) = D_{65}(l)\cdot R(l) \qquad (2)$$

From the tristimulus values, the 1931 CIE color coordinates x, y, z are defined as:

$$\begin{aligned} x &= X/(X+Y+Z) \\ y &= Y/(X+Y+Z) \\ z &= 1-(x+y) \end{aligned} \qquad (3)$$

All existing colors are represented in the x, y plane.

The relative luminosity A is a measure for the brightness of a surface as it appears to the human eye under certain illumination conditions. A white surface or a perfect mirror exhibits 100% relative luminosity, colored or grey surfaces less. In this sense, a colored or grey Lambertian surface is compared to a white Lambertian surface, and a specular reflecting surface is compared to the perfect mirror. The determination of the relative luminosity A is based on the photopic luminous efficiency function V(λ) and depends on the choice of the source. Again we employ the standard illuminant D_{65}, and the hemispherical reflectance R(λ):

$$A = \frac{\int R(l)\cdot D_{65}(l)\cdot V(l)dl}{\int D_{65}(l)\cdot V(l)dl} \qquad (4)$$

Given a calculated or measured spectrum of the hemispherical transmittance T(λ) of a sample, the solar transmittance T_{sol} is obtained by integration with the solar spectrum $I_{sol}(\lambda)$:

$$T_{sol} = \frac{\int T(l)\cdot I_{sol}(l)dl}{\int I_{sol}(l)dl} \quad , \qquad (5)$$

where usually the solar spectrum at air mass 1.5 (AM1.5) is used as intensity $I_{sol}(\lambda)$.

The solar reflectance R_{sol}, corresponding to the solar energy losses, can be defined analogously:

$$R_{sol} = \frac{\int R(l)\cdot I_{sol}(l)dl}{\int I_{sol}(l)dl}, \qquad (6)$$

where R(λ) is the simulated or measured hemispherical reflectance of the sample.

In the case of transparent thin film and substrate materials, absorption is absent and energy is conserved:

$$T(l) + R(l) = 1 \quad \text{and} \quad T_{sol} + R_{sol} = 1 \qquad (7)$$

The human eye perceives only a small part of the solar spectrum; large spectral regions in the ultraviolet and in the infrared are invisible. The basic idea is to create a surface, which reflects just a narrow frequency band in the visible range, thus giving rise to a colored appearance. For a colored solar collector, the nonreflected part of the solar spectrum should be completely converted to thermal energy. How bright will the colored reflection appear to the human eye, and how much energy will it cost? For a mathematical description we will consider an infinitely narrow spectral band, described by the Dirac delta distribution δ(x), with the property:

$$\int d(x-x_0)\cdot f(x)dx = f(x_0) \qquad (8)$$

for all functions f(x) .

In the considered case, the reflectance spectrum can be represented by the product of a constant and a delta distribution:

$$R(l) = C\cdot d(l-l_0), \qquad (9)$$

where λ_0 is the wavelength of the infinitely narrow spectral band. Using this reflectance spectrum, let us compute the relative luminosity A:

$$A = \frac{\int C d(\lambda - \lambda_0) \cdot D_{65}(\lambda) \cdot V(\lambda) d\lambda}{\int D_{65}(\lambda) \cdot V(\lambda) d\lambda} = \frac{C \cdot D_{65}(\lambda_0) \cdot V(\lambda_0)}{\int D_{65}(\lambda) \cdot V(\lambda) d\lambda} \quad (10)$$

The solar reflection R_{sol} is computed in a similar way:

$$R_{sol} = \frac{\int C d(\lambda - \lambda_0) \cdot I_{sol}(\lambda) d\lambda}{\int I_{sol}(\lambda) d\lambda} = \frac{C \cdot I_{sol}(\lambda_0)}{\int I_{sol}(\lambda) d\lambda} \quad (11)$$

At this point it is useful to introduce a figure of merit. We define the ratio of the relative luminosity A and the solar reflection R_{sol} as figure of merit M. Being large in the case of high relative luminosities or low solar energy losses R_{sol}, this number describes the energy efficiency of the visual perception ("brightness per energy cost"). Following this definition, we obtain:

$$M = \frac{A}{R_{sol}} = \frac{D_{65}(\lambda_0) \cdot V(\lambda_0)}{I_{sol}(\lambda_0)} \cdot \frac{\int I_{sol}(\lambda) d\lambda}{\int D_{65}(\lambda) \cdot V(\lambda) d\lambda} \quad (12)$$

This expression depends no longer on the constant C, it is independent of the intensity of the reflection. The integrals just correspond to a normalization, the dependence on the wavelength λ_0 is simple.

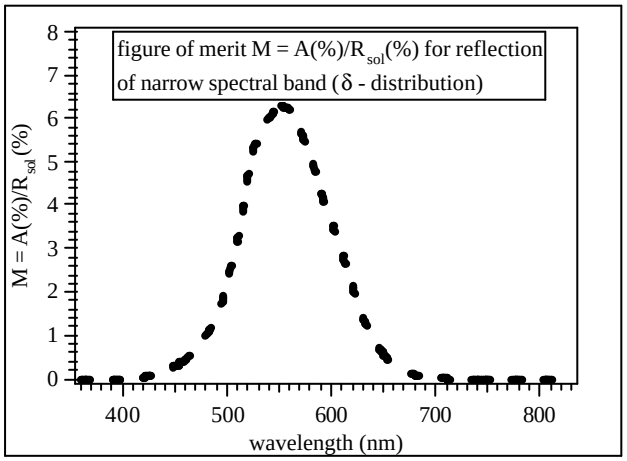

Fig.1: Figure of merit M , defined as the ratio of the relative luminosity A and the solar reflectance R_{sol} , computed for a narrow reflectance peak [a delta distribution $d(\lambda - \lambda_0)$], as a function of the peak position λ_0. The shape of this curve $M(\lambda)$, exhibiting a maximum at 550 nm (in the yellow green), is rather similar to the shape of the photopic luminous efficiency function $V(\lambda)$. However, the normalization is important: at the maximum, an absolute value of approximately six is reached.

The resulting curve is plotted in Fig.1. The shape of this curve, exhibiting a maximum at 550 nm (in the yellow green), is rather similar to the shape of the curve $V(\lambda)$. However, the normalization is important: at the maximum, an absolute value of approximately six is reached. What does this factor six mean? In this ideal case, a relative luminosity of 6 % costs only 1 % of the solar energy. If we desired a relative luminosity of 12 %, which is already considerable for a color (since 100 % corresponds to white), we would have to sacrifice only 2% of the incident energy. All possible reflection spectra can be approximated by a superposition of narrow spectral bands. Because the corresponding integrals are linear, the factor six represents the principal upper limit for M.

3. COMPUTATION OF THIN FILM INTERFERENCE

An optical multilayer of plane-parallel thin films on a substrate can be considered as a stratified medium. The propagation of electromagnetic waves in stratified media has been discussed by Born and Wolf (Born and Wolf, 1999). The field of optics of thin films has been reviewed by various authors (see e.g. Macleod, 2001, and refs. therein). Due to the multiple reflections between the different interfaces, the problem of the optical behaviour of a multilayered thin film stack is non-trivial. It can be treated, though, by the method of characteristic matrices, which defines one matrix M_r per individual layer (with the layer no. r). The whole layer stack is then represented by the matrix product. Let us take a look at this formalism.

Refraction at an interface is governed by Snell's law:

$$N_r \sin J_r = N_{r+1} \sin J_{r+1} \quad , \quad (13)$$

where the angles J_r are complex, and $N_r = n_r - ik_r$ is the complex refractive index of layer no. r with real part n_r and imaginary part k_r .

The idea of a tilted optical admittance h is introduced as follows:

$$h_r = \frac{N_r u}{\cos J_r} \quad \text{(for p – waves)} \qquad \text{or} \quad (14)$$

$$h_r = N_r u \cos J_r \quad \text{(for s – waves)} \qquad \text{respectively,} \quad (15)$$

using the admittance of free space υ (the ratio of the total tangential magnetic and electric fields in free space). Based on the concept of the optical admittance, the reflectance of an assembly of thin films can be calculated. In the following, h_0 means the tilted admittance of the

incident medium, and h_m the tilted admittance of the substrate. The multilayer is replaced by a single surface, which presents an admittance being the ratio of the total tangential magnetic and electric fields, C and B respectively, where

$$\begin{bmatrix} B \\ C \end{bmatrix} = \left\{ \prod_{r=1}^{q} M_r \right\} \begin{bmatrix} 1 \\ h_m \end{bmatrix} = \left\{ \prod_{r=1}^{q} \begin{bmatrix} \cos d_r & (i \sin d_r)/h_r \\ i h_r \sin d_r & \cos d_r \end{bmatrix} \right\} \begin{bmatrix} 1 \\ h_m \end{bmatrix}, \quad (16)$$

employing the phase shifts

$$d_r = 2\pi N_r d \cos J_r / \lambda \quad . \quad (17)$$

The order of multiplication needs to be respected. If q is the layer next to the substrate, then the order is

$$\begin{bmatrix} B \\ C \end{bmatrix} = [M_1][M_2]\ldots[M_q] \begin{bmatrix} 1 \\ h_m \end{bmatrix} \quad . \quad (18)$$

C and B thus obtained, we can compute the reflectance R(λ) and the transmittance T(λ):

$$R(\lambda) = \left(\frac{h_0 B - C}{h_0 B + C} \right) \left(\frac{h_0 B - C}{h_0 B + C} \right)^* \quad , \quad (19)$$

and

$$T(\lambda) = \frac{4 h_0 \, \mathrm{Re}(h_m)}{(h_0 B + C)(h_0 B + C)^*} \quad , \quad (20)$$

where * denotes the complex conjugate.

In spite of the apparent simplicity of the expressions, numerical calculations without some automatic aid are tedious in the extreme. Extended calculations are usually carried out by a computer. Multiple reflections between the two surfaces of a substrate are taken into account by summing up the contributions from each reflection. According to the coherence length of the considered light and the substrate thickness, coherence or incoherence have to be assumed, the latter holding for sunlight in combination with millimeter-thick substrates.

Numerous simulations of different interference filters with various refractive index and thickness combinations have been performed. Let us take a look at the following example: as optical model we assume a two layered coating on one side of a glass substrate (refractive index n = 1.52). The layer next to the substrate consists of a material with n = 2.2 (which corresponds roughly to e.g. vacuum deposited titanium dioxide), the topmost layer has a refractive index of 1.46 (which corresponds roughly to silicon dioxide).

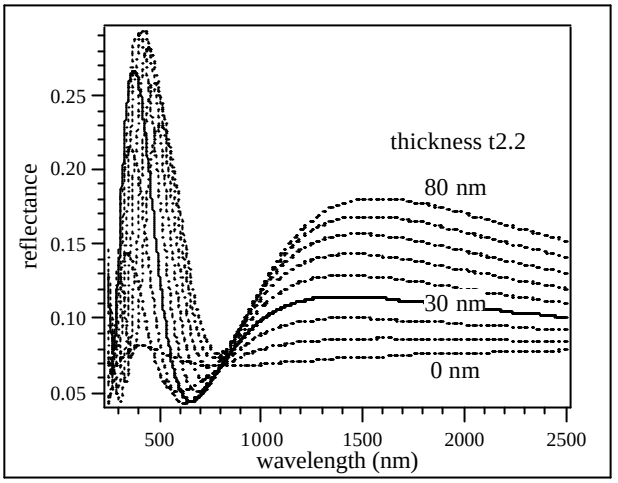

Fig.2: Simulated reflection spectra under normal incidence for a bilayered coating on glass (n = 1.52). Refractive indices of 2.2 and 1.46 have been assumed for the layer next to the substrate and the topmost layer, respectively. The thickness t2.2 of the high index material has been varied.

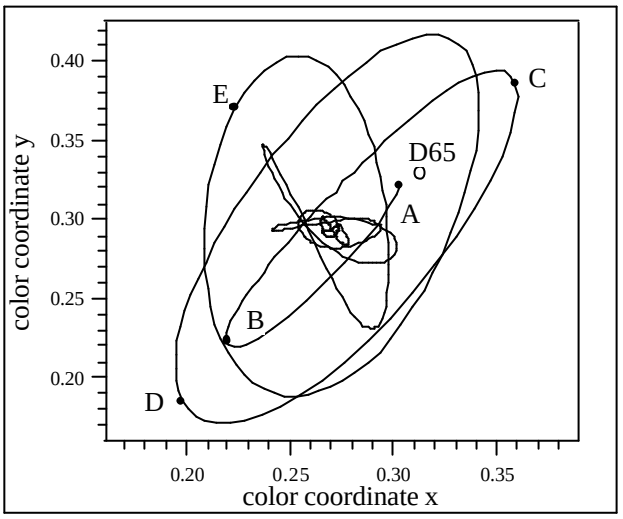

Fig.3: Trajectory in CIE x,y color space for the simulation shown in Fig.2. Each reflection spectrum yields a locus in color space. Curve parameter is the thickness t2.2 of the high refractive index layer (thickness t2.2 ranging from 0 nm to 1000 nm). The point A corresponds to t2.2 = 0 nm, point B to t2.2 = 30 nm. The letters C,D, and E denote points of high color saturation (yellow, blue-violet, and green). Point D65 corresponds to a white surface, illuminated by the CIE standard illuminant D65.

We compute the reflection under normal incidence. By variation of the film thickness t2.2 of the high refractive index material (n = 2.2) in steps of 10 nm, we obtain the curves plotted in Fig.2. The spectrum for t2.2 = 30 nm

exhibits especially interesting properties. A pronounced reflection peak yields a blue color, and for a wavelength region around 600 nm even an effect of anti-reflection is achieved. In the literature (Macleod 2001), this double layered coating is known as "V" coating (due to the shape of the reflection minimum). For each of the curves plotted in Fig.2, the CIE color coordinates x,y can be computed. Thus a trajectory in x,y color space results, with the thickness t2.2 as curve parameter (ranging from 0 nm to 1000 nm). This trajectory is depicted in Fig.3 (for an observer angle of 2°). The point A corresponds to t2.2 = 0 nm, the point B to t2.2 = 30 nm. As expected from Fig.2, the latter is located in the blue-violet. The letters C,D, and E denote points of high color saturation (yellow, blue-violet, and green). Fig.3 illustrates the complexity of the problem: even for a coating of only two layers, and under variation of only one parameter, the resulting trajectory is absolutely non-trivial. This implies the need of a global search strategy for suitable coating designs.

4. SOLGEL DIP-COATING

In SolGel dip-coating, a clean, plane substrate (e.g. a glass pane) is dipped into a solution and then withdrawn very regularly. A dynamical meniscus is formed, and the effects of solvent evaporation and gelation leave on both sides of the substrates a thin film of a xerogel. Film hardening and oxidation is commonly achieved by tempering at elevated temperatures in air. For a survey of techniques the reader might be referred to (Brinker and Scherer, 1990).

Often a certain parameter range can be found, where the formation of the liquid film follows the Landau-Levich equation (Landau and Levich, 1942):

$$h = 0.94 \cdot \frac{(h \cdot v)^{2/3}}{g_{LV}^{1/6} (r \cdot g)^{1/2}} \quad , \qquad (21)$$

with the liquid film thickness h, the withdrawal speed v, the viscosity h, the liquid-vapor surface tension g_{LV}, the density r, and the gravity g.

In this expression, the thickness of the liquid film is proportional to $v^{2/3}$. Solvent evaporation, gelation, and tempering, are commonly assumed to yield a coating thickness proportional to that of the liquid film.

Silicon dioxide and titanium dioxide films have been deposited on glass substrates from ethanol-based solutions containing the precursors tetraethyl-orthosilicate (TEOS) or tetraisopropylorthotitanat (TIOT). The substrates have been coated symmetrically on both sides. Given a solution of a certain concentration and viscosity, individual xerogel films have been deposited using different withdrawal speeds. By means of a baking procedure at elevated temperatures in air, these films have been hardened and oxidized. Optical transmission and reflection spectra for these samples have been measured in the VIS range (380 nm to 820 nm) by a spectrophotometer (ORIEL MS 125™ 1/8m Spectrograph, with Instaspec™ II Photodiode Array Detector). Film thickness and refractive index have been extracted from these optical data by a numerical fitting procedure (formulae according to section 2). The film thickness of TiO_2 films vs. the withdrawal speed is displayed in Fig.4. A power law could be easily fitted to these data, yielding an exponent of 0.67+/-0.05, in perfect accordance with what we expected from the Landau-Levich equation (21). For the SiO_2 films, results have been rather similar. Within a certain parameter range, a power law with an exponent of 2/3 could be confirmed.

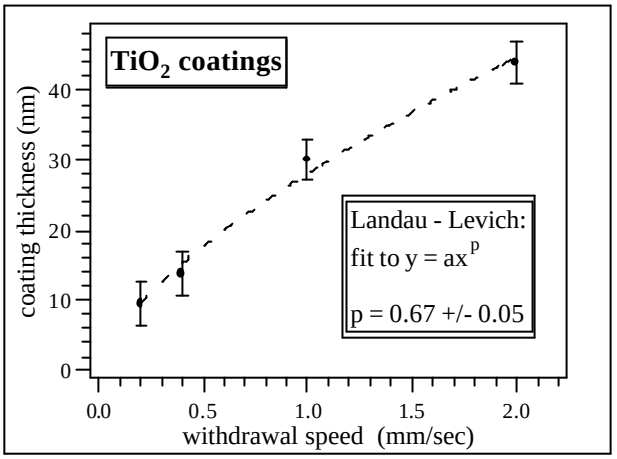

Fig.4: Thickness of SolGel deposited TiO_2 films as a function of withdrawal speed. The data could be easily fitted by a power law with the exponent of 0.67+/-0.05, in perfect accordance with the Landau-Levich equation (22).

Once the relation of film thickness and withdrawal speed is known, well defined multilayered coatings can be deposited, controlling the thickness of the individual layers. As an example, we show the realization of the bilayered V coating already mentioned in section 2 (see also Fig.2). First we defined the target: we simulated the transmission spectrum for glass substrate coated on each side by the same bilayer. As derived from the spectrophotometric data, refractive indices of 1.47, 2.1 and 1.52 have been assumed for the silicon dioxide thin films, the titanium dioxide thin films, and the glass substrates, respectively. Film thicknesses of 125 nm (silicon dioxide) and 27 nm (titanium dioxide) have been chosen. Withdrawal speeds have been s et according to the known relations to the film thickness. Two dip-coating steps have been performed successively, with an

annealing procedure following each xerogel deposition. The transmission spectrum of the fabricated sample matches very closely the desired target spectrum (Fig.5). Various samples with different thickness combinations have been checked successfully. Obviously, no perturbing effects, such as excessive mixing at the interface, or different flow behavior on different surfaces, occurred. Therefore, we believe that even multilayers of higher complexity can be designed and deposited in a controlled manner.

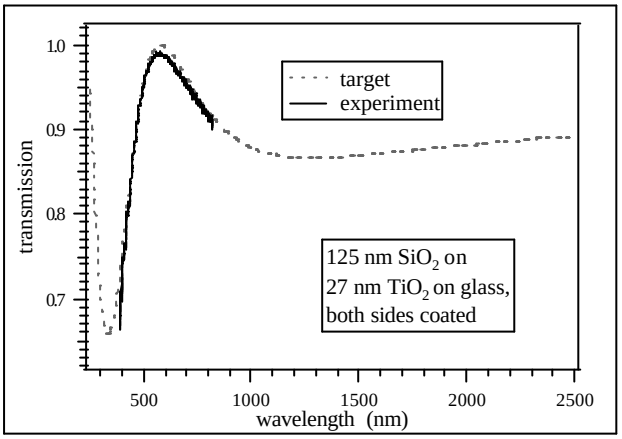

Fig.5: Transmission of a glass substrate coated on both sides by a bilayer (125 nm SiO_2 on 27 nm TiO_2). The experimental spectrum matches closely the designed target.

5. REACTIVE MAGNETRON SPUTTERING

Single and multilayered coatings of SiO_2, TiO_2, and Al_2O_3 have been deposited by reactive magnetron sputtering in a vacuum chamber, which can be pumped down to a base pressure of $1*10^{-6}$ mbar using turbomolecular pumps in combination with a liquid-nitrogen cooling trap. For alternating deposition of multilayers, two water-cooled magnetrons, carrying Si, Ti, or Al targets, are driven by radio frequency (RF) power at 13.56 MHz, or by bipolar pulsed power in a range from 50 to 250 kHz. During thin film deposition, the substrate faces the target at a distance of several centimetres. Substrates can be heated resistively, a temperature measurement is provided by thermocouples. Argon and oxygen are fed into the chamber via two mass flow controllers. By throttling the pumping system, a working pressure around $5*10^{-3}$ mbar is adjusted. Under these conditions, a stable glow discharge is sustained. A Kaufman-type ion source enables a substrate pre-treatment by Ar sputtering. In order to achieve reproducible and stable deposition conditions, the plasma process is always operated for some minutes with the chosen parameters (gas mixture, total pressure, input power), before finally coating the substrate. As substrate materials, glass AF45 and silicon wafers have been chosen. In-situ photoelectron spectroscopy gives information on the chemical composition and on electronic properties of the deposited films. The electron spectrometer is equipped with a hemispherical analyser (Leybold EA 10/100 MCD), a He resonance lamp for valence band spectroscopy (excitations: He I, He II), and an X-ray source for core level spectroscopy (Mg-Kα radiation). For details see e. g. (Schüler et al., 1999). Simultaneously to the film deposition, data can be acquired by laser reflectometry. As light source we use a solid state laser at a wavelength of 532 nm with 1 mW power and a beam diameter of 1 mm (Laser Compact, model LCM-T-01ccs). The measurement technique includes chopper, photodiodes, and lock-in amplifiers for the sampling of monitor and probe beams. A polarization filter is used to choose a well defined polarization direction of the laser light. The angle of reflection is determined accurately by triangulation [details in (Schüler et al., 2000)]. Spectroscopic ellipsometry is used to determine the thickness and the optical properties of individual films on Si substrates (instrument: SENTECH SE 850). Often, a dispersion relation (e.g. a Cauchy formula) is assumed to numerically fit data of the ellipsometric angles psi and delta. Transmission and reflection spectra of the coated glass substrates are measured in the UV-VIS-NIR range by means of a Varian CARY05 spectrophotometer.

A very good stability of the deposition could be achieved. Data of real-time laser reflectometry of the growth of a TiO_2 film on a silicon wafer are shown in Fig.6. The angle of reflection was 52.5° +/- 0.5°, and the laser light was polarized parallel to the plane of reflection. The theoretical formula [see Eqs. (14) to (20)] can be fitted perfectly to these data, yielding the index of refraction (n = 2.37), the extinction coefficient (k = 0.0), and the deposition rate (r = 0.060 nm/sec). The strength of this method lies in the fast access to the deposition rate and optical properties (at the given wavelength), without even opening the chamber or taking the samples out.

In contrast to laser-based methods, spectroscopic ellipsometry is a versatile tool providing information on the dispersion relation in a quasi-continuous wavelength range. The film thickness and thus the deposition rate are extracted at the same time by a numerical data analysis. As an example, let us consider a thin film of SiO_2 deposited on a silicon wafer. We measured the ellipsometric angles psi and delta for various angles of reflection (40°, 50°, 60°, and 70°). The experimental results are displayed in Fig.7. These data are analysed on the basis of an optical model. The optical properties of the individual thin film are assumed to follow a Cauchy dispersion relation. The numerical fitting procedure yields the function $n(\lambda)$ shown in Fig.8, the extinction coefficient k = 0 (within the considered wavelength range), and a film thickness of 154 nm.

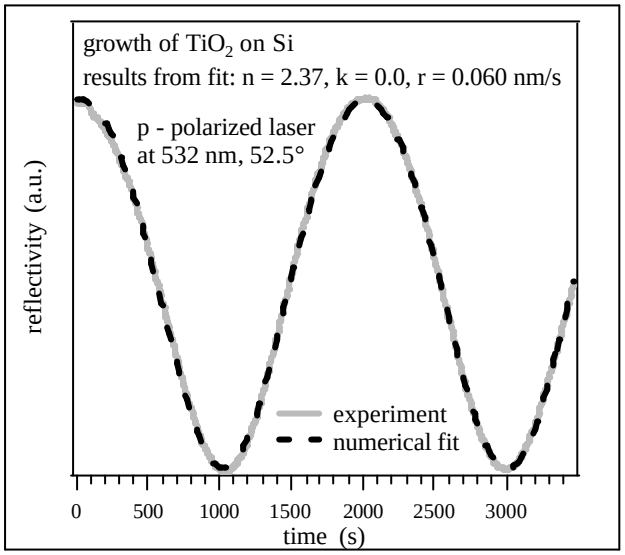

Fig.6: Real-time laser reflectometry. Data have been acquired simultaneously to film growth and are perfectly fitted by the theoretical formula. The numerical fit yield the optical properties n and k at the laser wavelength 532 nm, and the deposition rate, thus the total thickness of the finally formed film.

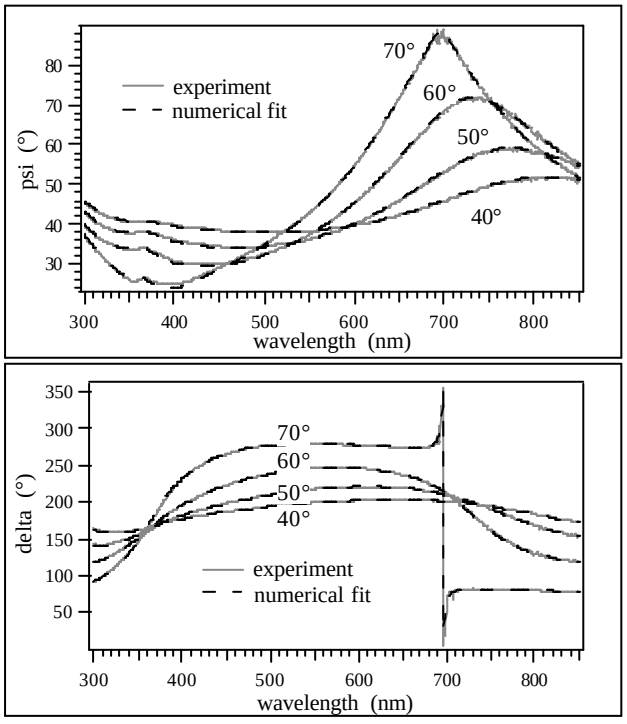

Fig.7: Spectroscopic ellipsometry of a SiO_2 film on a silicon substrate. The experimental data on the ellipsometric angles psi and delta have been fitted by a Cauchy dispersion relation.

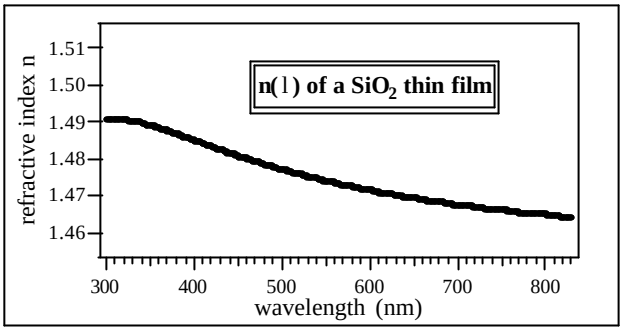

Fig.8: The refractive index n(l), as inferred by numerical analysis of the ellipsometric data shown in Fig.8. An extinction coefficient k of zero (within the considered wavelength range), and a film thickness of 154 nm have been found.

In preliminary experiments, various multilayered coatings on glass substrates have been fabricated. As thin film materials, SiO_2, Al_2O_3 and TiO_2 have been used. The optical methods of real-time laser reflectometry, and spectroscopic ellipsometry, provide the knowledge on deposition rates and optical constants. Thus, the multilayers can be produced in a controlled manner. Spectrophotometric measurements on these samples yield promising values of the solar transmission, the relative luminosity, and thus the figure of merit M. A considerable variety of different reflection colors could be obtained.

6. DISCUSSION

The figure of merit M turned out to exhibit a principal upper limit of value six, meaning a large potential in the ideal case: for example, twelve percent relative luminosity costs only two percent of solar transmission. Twelve percent relative luminosity represents already a considerable value for a colored, non-white surface, while two percent reflection losses can be regarded as moderate, compared to the reflection losses of an uncoated glass pane (≈ 8 %). In contrast to photovoltaic systems, where cell area is precious, the surface area of the thermal collectors generates only a fraction of the total system costs (the total system including pumps, boiler, stock, tubing etc.). Therefore, for solar thermal systems, the loss of some percent in transmission can more easily be compensated by a larger receiving area. A colored glazing hiding the absorber structure would promote facade integration of solar thermal systems. Vertical facade collectors are especially advantageous for the winter season, when the sun is closer to the horizon and thermal energy is needed. Additionally, vertical facade collectors are less exposed to the sun during summertime and thus better protected against

overheating. Collector area could thus be dimensioned more generously.

When applying any coating process, care has to be taken to achieve a superior film homogeneity, which is essential for interference filters. Vacuum processes yield in general high quality films, but a considerable investment into the vacuum coating machines is necessary already in the start-up phase. The scale-up of a vacuum process, which has been developed in the laboratory, is possible, but non-trivial (Milde et al., 2000). This is much easier for SolGel dip-coating. Once the right solution and withdrawal speeds are found, the size of the glass pane does not alter the basic process parameters. Here, the main problem is to avoid dust, which creates defects and harms the coating quality. Costs rise with the repeated baking of multilayered coatings on large glass panes. One promising option could be special precursors, which enable a film hardening by ultraviolet light (Menning et al. 1999).

7. CONCLUSIONS

The general potential of colored thermal solar collectors is promising, and can be expressed by a figure of merit M defined as the ratio of the relative luminosity A and the solar energy losses by reflection R_{sol} . The principal upper limit for this figure M amounts to the value six, meaning low energy costs per perceived brightness. Aiming an energy-efficient coloration of the collector glazing, multilayered optical coatings are simulated and designed with computer aid. The SolGel method and magnetron sputtering processes, both with their specific advantages and disadvantages, can be used to fabricate these coatings. Optical measurement techniques, such as real-time laser reflectometry, spectroscopic ellipsometry, and spectrophotometry, are helpful tools for the realization of such interference filters.

ACKNOWLEDGEMENTS

Financial support of this work has been provided by the Swiss Federal Office of Energy SFOE and by the Swiss National Science Foudation. Authors are grateful to Dr. I. Hagemann, and Dr. P. W. Oliveira for inspiring discussions, and to R. Steiner for the technical support.

REFERENCES

Hestnes A.G. (1999). *Sol. Energy* 67, Issues 4 – 6, 181

Roecker C., Affolter P., Bonvin J., Gay J.-B., Müller A.N. (1995). *Sol. Energy Mater. and Sol. Cells* 36, 381

Hagemann I.B. (2002) *Architektonische Integration der Photovoltaik in die Gebäudehülle*, PhD thesis, ISBN 3-481-01776-6, Müller, Köln

Scartezzini J.-L., Courret G. (2002). *Sol. Energy* 73 (2), 123

Graf W., Brucker F., Köhl M., Troscher T., Wittwer V., Herlitze L. (1997). *J. of Non-crystalline Solids* 218, 380

Schüler A., Videnovic I.R., Oelhafen P., Brunold S., (2001). *Sol. Energy Mater. and Sol. Cells* 69**,** 271

Lazarov M., Raths P., Metzger H., Spirkl W. (1995). *J. of App. Phys.* 77, 2133

Tabor H., U.S. Patent 2,917,817 (1955)

Kaluza L., Orel B., Drazic G., Köhl M. (2001). *Sol. Energy Mater. and Sol. Cells* 70, 187

Orel Z.C., Gunde M.K. (2001). *Sol. Energy Mater. and Sol. Cells* 68, 337

Tripanagnostopoulos Y., Souliotis M., Nousia T.(2000). *Sol. Energy* 68, 343

Macleod H.A. (2001) *Thin-Film Optical Filters*, Institute of Physics Publishing, Bristol and Philadelphia

International Commission on Illumination CIE (1986), *Colorimetry*, CIE Publication 15.2., 2nd Ed., ISBN 3-900-734-00-3, Vienna

Born M. and Wolf E. (1999) *Principles of Optics*, 7th Ed., Cambridge University Press

Brinker, C.J., Scherer, G.W. (1990) *Sol-Gel Science*, Academic Press, Boston

Landau L.D., Levich, B.G. (1942), *Acta Physiochim* 17, 42, U.R.S.S.

Schüler A., Gampp R., Oelhafen P. (1999). *Phys.Rev. B* 60(23), 16164

Schüler A., Ellenberger C., Oelhafen P., Haug C., Brenn R. (2000). *J. of Appl. Phys.* 87, 4285

Milde F., Dimer M., Hecht C., Schulze D., Gantenbein P. (2000). *Vacuum* 59(2-3), 825

Mennig M., Oliveira P.W., Schmidt H. (1999). *Thin Solid Films* 351(1-2), 99